



Isotherms, kinetics and thermodynamics of industrial dye acid red 27 adsorption on Sugarcane Bagasse Ash

Joana Eliza de Santana¹ · Fábio Gabriel Silva de Andrade¹ · Aldebarã Fausto Ferreira² · Marcos Gomes Ghislandi³ · Maurício Alves da Motta Sobrinho¹

Received: 22 September 2023 / Accepted: 2 January 2024 / Published online: 11 January 2024
© The Author(s), under exclusive licence to Springer-Verlag GmbH Germany, part of Springer Nature 2024

Abstract

In this study, sugarcane bagasse ash (SCBA), obtained as residue from the sugar mill, was used as an adsorbent for Acid Red 27 (AR27) removal from aqueous solutions. The ash characterization data showed 23.63% of organic compounds and silica (α -SiO₂) as the most expressive inorganic compound (confirmed by X-ray diffractogram), the BET surface area had a value of 62.79 m².g⁻¹ and the pH_{pzc} was 8.45. Regarding the adsorptive tests, the optimal initial pH to the dye removal was 2.0. The adsorption equilibrium reached in about 4 h contact time and optimum SCBA dosage was found to be 4 g.L⁻¹. The pseudo-second order model best represented the adsorption kinetics. The Freundlich equation presented the best fit to the equilibrium data for the removal of AR27 by ash, with maximum adsorption capacity of 15 mg.g⁻¹ at pH 2.0. Thermodynamic study indicate that AR27 adsorption on SCBA occurs through a physisorption mechanism, with $\Delta H^{\circ}_{ads} < 15$ kJ.mol⁻¹. The ΔH°_{ads} evaluated by Vant' Hoff equation was explained as a combination of water desorption enthalpy, ΔH°_w and isosteric like enthalpy, ΔH°_D for the dye adsorption in liquid environment. The $\Delta H^{\circ}_D = 9.2$ kJ.mol⁻¹ was calculated from Clausius-Clapeyron approach. The effects of coexisting anions on the adsorption and regeneration and reuse of the adsorbent were also investigated. This study suggests that SCBA, which was used without any pretreatment, has the potential to be applied as a low-cost adsorbent to mitigate effluents contamination with AR27 dye at low concentrations.

Keywords Dye adsorption · Decontamination · Sustainability · Adsorption kinetics · Isotherms · Sugar mill waste · Isosteric enthalpy

Responsible Editor: Tito Roberto Cadaval Jr

Highlights

- Acid Red 27 dye adsorption at sugarcane bagasse ash (SCBA) has been investigated.
- Isosteric enthalpy analogy for adsorption in liquids was applied to better understanding the thermodynamic parameters.
- Regeneration of SCBA with NaOH (0.1 and 0.3 M) allowed recuperation of at least 75 % of the dye adsorbed.
- Adsorption with coexisting anions evidenced high influence of bicarbonate for decrease the SCBA adsorptive capacity.

✉ Joana Eliza de Santana
joana.santana@ufpe.br

¹ Chemical Engineering Department, Federal University of Pernambuco, Recife, PE 50.740-590, Brazil

² Department of Fundamental Chemistry, Federal University of Pernambuco, Recife, PE 50.740-590, Brazil

³ Engineering Campus, Federal Rural University of Pernambuco, Cabo de Santo Agostinho, PE 54518-430, Brazil

Introduction

Brazil is the world's largest producer of sugarcane (FAOSTAT 2023), an extremely versatile product, and major player in the sugar-energy sector. It is estimated that sugarcane production in the harvest of 2022/2023 has reached 610.1 million tons (CONAB 2023a). In that same harvest, alcohol production totaled 27.3 billion liters, with 15.7 billion of the hydrated type, and 11.6 billion of the anhydrous type. The sugar production was 37 million tons; where, of this total, 27.7 million were exported (CONAB 2023b). This performance confirms the importance of sugarcane as a national commodity, placing Brazil as the second largest producer of ethanol and the largest producer of sugar.

In the sugar and alcohol industry, bagasse is generated in large quantities, approximately 25 a 30% of the weight of the total sugarcane crushed (Gar et al. 2017; Souza et al. 2011). This biomass is burned in high-pressure boilers to generate steam and electricity, making some industries self-sufficient

in energy and offering the possibility of selling the surplus. The bagasse burning process generates sugarcane bagasse ash (SCBA) as a residue, which, if not disposed correctly, would be a serious environmental problem. By weight, it is estimated that SCBA corresponds to 0.6% of the weight of processed sugarcane (Andrade Neto et al. 2021; Matos et al. 2021). Leading the Brazilian industry to allocate 3.7 million tons of ash in the 2022/2023 harvest.

Presenting a high silica content, SiO_2 , bagasse ash has been widely studied for construction purposes, such as, a mineral additive in the manufacture of cements and ceramics, in the manufacture of reinforced concrete (in order to reduce corrosion by chlorides), as well as in the preparation of pastes and mortars (Patel 2020). Other studies have shown that ash can also be used in the production of adsorbents, mesoporous silica, zeolites, immobilizers in reactors and secondary abrasives (Patel 2020; Sriatun et al. 2018; Rahman et al. 2015).

Furthermore, the use of ash as an adsorbent can be a very promising alternative, especially since it is cheap, readily available and with potential application by the industry as an input or product to mitigate impacts generated by contaminated effluents (Mane et al. 2007; Mall et al. 2005, 2006; Gupta et al. 2000).

Dyes have been widely used in various industrial fields, such as pharmaceutical, textile, cosmetics, food, pulp and paper, photographic etc., and their disposal must be constantly monitored. The presence of dyes in natural waters inhibits the penetration of sunlight, reducing the photosynthetic reaction and interfering with the biological degradation of water impurities, resulting in ecological imbalance. Furthermore, some may be toxic and even carcinogenic or mutagenic (Ebrahimpoor et al. 2019; Pinedo-Hernández et al. 2012).

Several technologies have already been proposed for the removal of dyes from water, such as electrochemical methods, chemical precipitation, advanced oxidation processes, biological treatment and membrane filtration (Arabkhani et al. 2021). As synthetic dyes have a complex aromatic structure, they are rarely removed by biological methods due to their low biodegradation (Salman-Naeem et al. 2018). On the other hand, combined techniques sometimes show good performance in color removal, but most have high costs, high technical requirements and complicated practice. In addition, some of them cause the treated effluent to remain with high values of organic carbon dissolved due to resulting by-products, which can be more toxic than the previous molecule (Metivier-Pignon et al. 2007; Nassar 2010). In fact, adsorption is seen as a simple technique, with excellent cost-effectiveness, ease of operation when using efficient and widely available adsorbents, which is why it has been widely studied and industrially applied (Arabkhani et al. 2021; Ebrahimpoor et al. 2019).

The dye Acid Red 27 (AR27) has wide industrial applications, being used in household products and cosmetics, to dye synthetic and natural fibers, leather, wood, paper, and in photography (Chhabra et al. 2015). However, the specialized literature shows few studies on its decontamination in water (Nassar 2010; Al-Aoh et al. 2013; Salman-Naeem et al. 2018; Ebrahimpoor et al. 2019; Yusof et al. 2020), and no study was found in our research on its adsorption in sugarcane bagasse ash.

The objectives of this work are to characterize the ashes obtained from the combustion of sugarcane bagasse in high-pressure boilers and to study the adsorption of the dye AR27 by the SCBA. The applicability of kinetic and isothermal models was evaluated, determining the influence of adsorbent dosage, initial pH, and the presence of anions on its adsorption capacity. The temperature influence on adsorption isotherms was studied an applied for understanding the thermodynamic parameters and the isosteric enthalpy behavior of the dye adsorption in SCBA. The study of its regeneration and reuse was also carried out.

Experimental

The chemicals used in this study were hydrochloric acid P.A. (37%, Quimica Moderna, Brazil), sodium hydroxide P.A. (> 98%, Dinâmica, Brazil), sodium chloride P.A. (> 99.5%, Fmaia, Brazil), anhydrous sodium sulfate P.A. (> 99.0%, Vetec, Brazil), sodium bicarbonate P.A.-ACS (> 99.7% Química Moderna, Brazil), and the dye acid red 27 (Polycrom, Brazil). All chemicals were used without further purification.

Sugarcane bagasse ash

The ashes used to this work was kindly provided by Petribu S.A. sugarcane mill (Lagoa de Itaenga, PE, Brazil). Through the industrial process, the sugarcane bagasse was burned in high-pressure boilers at 380 °C, resulting in ashes that falls in a water channel, which was dragged to a settling pool. After its draining, the SCBA were collected, dried at 105 °C for about 24 h. Then, it was sieved, and the part with particle size lower than 0.25 mm was used as adsorbent.

Adsorbate

The synthetic dye Acid Red 27 [CAS 915–67-3, C.I. 16185, chemical formula = $\text{C}_{20}\text{H}_{11}\text{N}_2\text{Na}_3\text{O}_{10}\text{S}_3$, molecular weight = $604.5 \text{ g}\cdot\text{mol}^{-1}$, $\text{pK}_a = 6.5$, $\lambda_{\text{max}} = 520 \text{ nm}$ (Fig. S1)]. A quantity of dye was weighed in a Quimis Q500B210C analytical balance and dissolved in distilled water to prepare a stock solution of $1000 \text{ mg}\cdot\text{L}^{-1}$. Experimental solutions at the desired concentration were obtained by successive

dilutions with distilled water. The structure of the AR27 is illustrated in Fig. 1.

Characterization of the sugarcane bagasse ash

The chemical composition of SCBA was determined by X-ray fluorescence (XRF), using a Rigaku ZSX Primus II equipped with Rh tube and 7 analyzer crystals. Scanning electron microscope (SEM) images were obtained with a VEGA3 (Tescan, CZ) Microscope, operating at acceleration voltage from 5 to 20 kV. Each sample was placed on a small metallic support (stub) with double-sided carbon tape. The samples were then metallized with a nanometric layer of gold using a Desk V (Denton Vacuum, US). The thermogravimetric curve was obtained in an instrument TGA Q50 V6.7 Build 203 and performed in the range of 27 to 1000 °C with a flow of air and a heating rate of 10°C/min. The N₂ adsorption–desorption isotherms were obtained at 77 K and relative pressures up to 0.01, using a Quantachrome Instruments NOVA STATION A. The specific surface area (SBET) of the adsorbent was calculated from the adsorption data using the Brünauer-Emmett-Teller (BET) method. The micropore area and volume (S_{mic} and V_{mic}) were obtained by the t-plot method. The mesopore volume (V_{ext}) was calculated as the difference between the total pore volume (V_T) and the micropore volume (V_{mic}), obtained at $P/P_0 = 0.99$. X-ray diffraction (XRD) patterns were obtained using a Shimadzu XRD-6000 instrument operated with Cu-K α radiation ($\lambda = 0.1546$ nm) in the 2θ range from 5 to 80°, with voltage and current of 30 kV and 30 mA, respectively. FTIR spectra were recorded from 4000 to 400 cm⁻¹ using

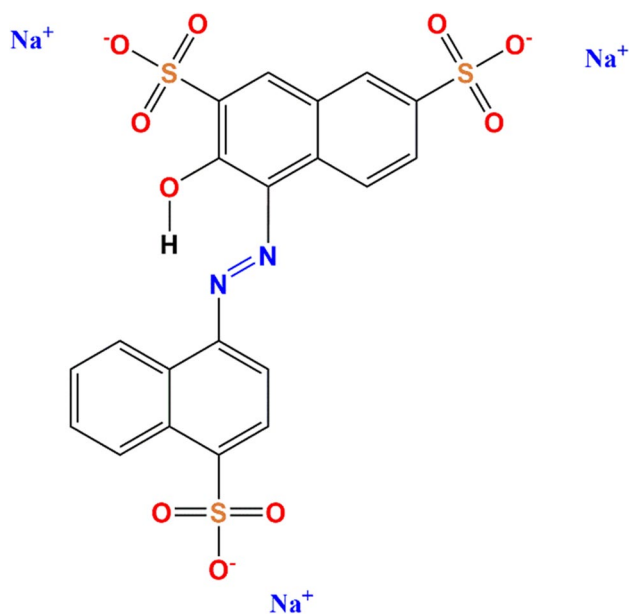


Fig. 1 Molecular structure of Acid Red 27

a Shimadzu IR PRESTIGE-21 spectrometer. The point of zero charge (pH_{pzc}) of the adsorbent was obtained according to an adapted methodology (Mahmood et al. 2011), using NaCl (0.1 M) saline solution and adjusting the initial pH (pH_0) with solutions of HCl (0.1 M) or NaOH (0.1 M). The pH was monitored using a pHmeter Instrutherm PH-1500.

Adsorption experiments

To study the adsorption of the AR27 dye using SCBA as adsorbent, experiments in batches were conducted in a shaker (Marconi MA-420) at 30 ± 1 °C. For each experimental run, 25 ml of dye solution of known concentration and a measured amount of adsorbent were placed in 125 ml Erlenmeyer flasks, under stirring speed of 300 rpm. At the end of each experiment, the samples were centrifuged to separate the adsorbent and the final concentrations determined using a UV–visible spectrophotometer (Thermo Fisher Scientific Genesys 10-S) at a wavelength of 520 nm.

For kinetic experiments, the contact time ranged of 5–360 min with dye solutions concentration of 30 mg.L⁻¹. The models evaluated in this work were Pseudo-first-order (PFO), Pseudo-second-order (PSO), Elovich and Intraparticle Diffusion (IPD, proposed by Weber and Morris). The equations are given in Table S1.

The effect of important parameters that influence adsorption was studied. The effect of initial pH (pH_0) on dye removal was studied over a pH range of 2 to 12. The pH_0 was adjusted by adding dilute aqueous solutions of HCl (0.1 M) or NaOH (0.1 M). The effect of adsorbent dosage on dye removal percentage and adsorption capacity was analyzed by changing the adsorbent dosage from 1.2 to 12 g.L⁻¹, keeping other factors unchanged. To define the adsorbent dosage, a dye solution with a defined concentration (30 mg.L⁻¹) was placed in contact with different amounts of adsorbents (0.05 g to 0.8 g) until equilibrium was reached.

For equilibrium experiments, different dye concentrations ranging from 2.5 to 240 mg.L⁻¹ (2.5; 5; 20; 40; 50; 60; 80; 100; 120; 140; 160; 180; 200; 220; 240 mg.L⁻¹) were used. The vials were placed on a shaker until equilibrium was reached. The experimental data were fitted to the Langmuir, Freundlich and Temkin models, considering linear and non-linear fits. The equations are given in Table S2.

The non-linear fitting to the data was performed in Origin Pro©. Chi-square tolerance value of 1.0×10^{-9} (difference between reduced chi-square values of two successive iterations) was used as the convergence criterion.

Thermodynamic evaluations were carried out at temperatures of 303, 321 and 338 K using the incubator shaker, for dye concentrations ranging from 20 to 200 mg.L⁻¹ (20; 40; 60; 80; 100; 120; 140; 160; 180; 200 mg.L⁻¹).

In addition, the effects of coexisting anions (Cl^- , SO_4^{2-} , HCO_3^-) at concentrations of 0.1 M on AR27 adsorption

by SCBA were investigated. The salts (NaCl, Na₂SO₄, NaHCO₃) were added separately to the dye solution at a defined concentration (30 mg.L⁻¹) until equilibrium was reached.

For the regeneration and reuse of the adsorbent, 0.1 g of the SCBA was added into 25 mL of 30 mg.L⁻¹ dye solution (pH₀ = 2) and placed under constant stirring (300 rpm) at 30 ± 1 °C for 4 h. The final concentration was measured and the adsorbent was separated by centrifugation. Alkaline solutions are used to elute negatively charged dyes; alkaline eluent sodium hydroxide solution are most used for desorption study to elute anionic dye (Patel 2021). So, the regeneration possibility of exhausted adsorbent was investigated using distilled water and NaOH solution at different concentrations (0.01 M, 0.1 M and 0.3 M). The adsorbent used was added into 10 mL of eluent in a shaker (300 rpm stirring) for 2 h at 30 ± 1 °C; after that, the SCBA was washed with distilled water to neutral pH to remove the residual NaOH. The regenerated adsorbent was tested for AR27 adsorption (initial dye concentration: 30 mg.L⁻¹; pH₀ = 2; contact time: 4 h; adsorbent dosage: 4 g.L⁻¹; temperature: 30 ± 1 °C). The SCBA adsorbent was regenerated by three cycles. The amount of AR27 adsorbed after the cycles was analysed and recorded.

All experiments were performed in duplicate.

The removal efficiency (%) of dye was calculated using the Eq. 1. The adsorption capacity, q_e (mg.g⁻¹), was calculated from the mass balance (Eq. 2) after the attainment of equilibrium.

$$\text{Removal efficiency} = \frac{(C_0 - C_e)100}{C_0} \quad (1)$$

$$q_e = \frac{(C_0 - C_e)V}{W} \quad (2)$$

where C₀ (mg.L⁻¹) is the initial concentration, C_e (mg.L⁻¹) is the equilibrium sorbate concentration, V is the volume of the solution (L) and w is the mass (g) of the adsorbent.

Results and discussion

Characterization of the sugarcane bagasse ash

Ash, in general, has a very high concentration of silica and contains aluminum, iron, alkali and alkaline earth metal oxides as minor components (Teixeira et al. 2008). Table 1 shows the results of XRF analysis of SCBA sample along with its chemical composition. The results indicate that SCBA mainly contains SiO₂ (52.40%), CaO (5.26%), K₂O (5.00%), Fe₂O₃ (4.09%), among other minor constituents. SiO₂ is the major component of SCBA, being consistent

Table 1 Chemical constituents (%) of SCBA determined by XRF

Chemical constituent	(%)
SiO ₂	52.404
CaO	5.262
K ₂ O	5.002
Fe ₂ O ₃	4.086
P ₂ O ₅	3.979
MgO	2.100
SO ₃	1.298
Na ₂ O	0.993
TiO ₂	0.519
Cl	0.275
MnO	0.206
ZnO	0.053
SrO	0.046
BaO	0.046
CuO	0.031
ZrO ₂	0.031
Cr ₂ O ₃	0.023
RbO	0.015
As ₂ O ₃	0.008
LOI	23.632

with results obtained conventionally for sugarcane ashes (Patel 2020; Zhang et al. 2020; Patil et al. 2021). Variations in ash composition are related to differences in the chemical composition of the soil and the variety of cultivated sugarcane.

The SEM images of the SCBA are shown in Fig. 2. The porous morphology of SCBA may be due to inherent structure in the original raw material, the sugarcane bagasse, which mainly contains cavities on its fiber composition. A large number of fiber-like macrostructures are also seen in the micrograph (Fig. 2a). At a higher magnification (Fig. 2b), it is possible to observe irregular micro-sized particles with round open pores, similar to that observed for activated carbon (Deng et al. 2021; Gan 2021). SEM analysis at higher magnification was carried out to show in more details the nano-micro structure of the SCBA (Fig. S2).

In Fig. 3, in which the XRD pattern is displayed, it can be observed an overall amorphous behavior of the ashes, characterized by a broad peak at a maximum of 23°. There is also a crystalline character, indicated by the peak at 26.7°, and others small peaks. These reveal the presence of quartz (α-SiO₂) as the predominant crystalline material. This information is consistent by the chemical analysis of XRF, which indicates silicon as an element present in high quantity, and with other works (Patel 2020; Ribeiro and Morelli 2014).

The porosimetry characterization of the SCBA (Table 2) shows a BET specific surface area of 62.79 m².g⁻¹, a small value, but it must be taken into account that the ashes did not undergo activation processes. The average pore diameter

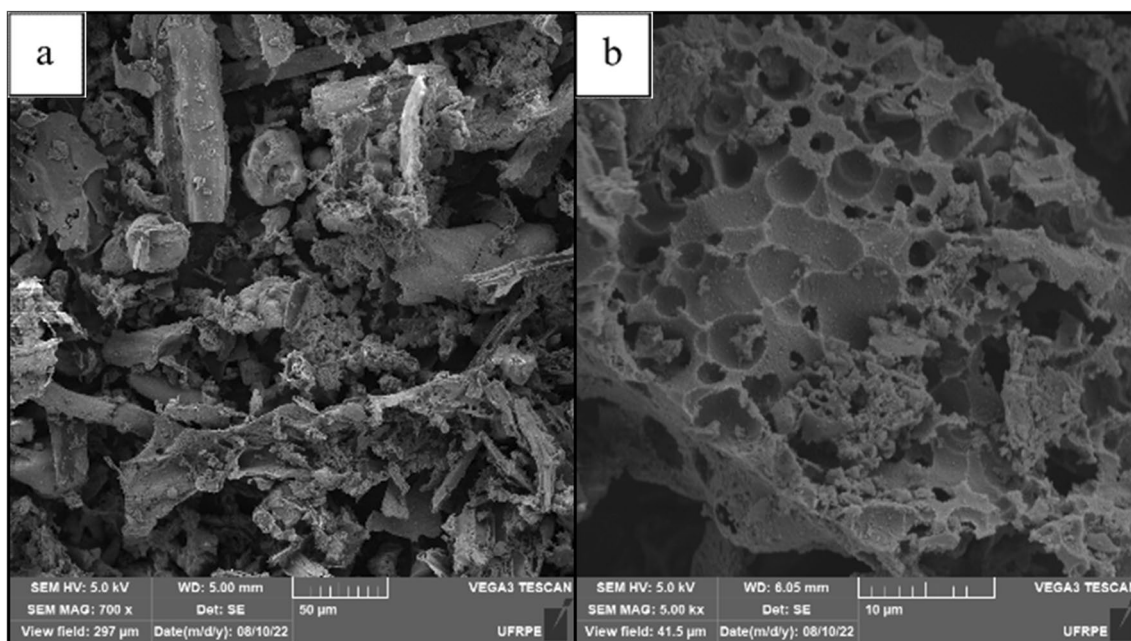


Fig. 2 Scanning electron microscopy of SCBA with magnification: a) 700 x; b) 5000 x

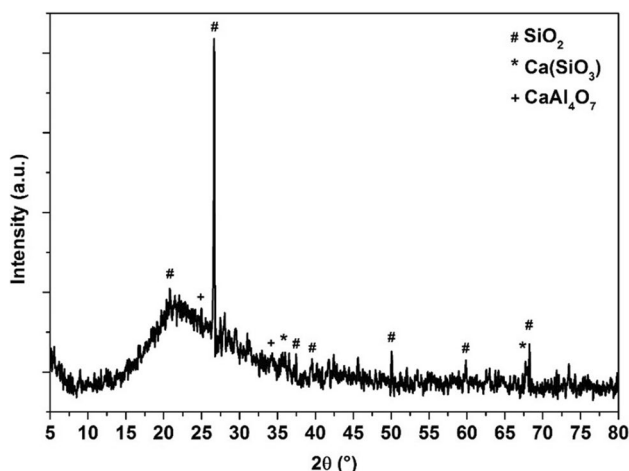


Fig. 3 X-ray diffraction pattern of SCBA

Table 2 Data for the pore structure properties of the sugarcane bagasse ash

BET specific surface area ($\text{m}^2 \cdot \text{g}^{-1}$)	62.79
Total pore volume for pores with Diameter less than 261.13 nm at $P/P_0 = 0.992609$ ($\text{cm}^3 \cdot \text{g}^{-1}$)	0.05283
Average pore diameter (nm)	3.366

calculated was 3.37 nm, classified, according to IUPAC, as mesoporous (Rouquerol et al. 1994).

In Fig. 4, the FTIR spectrum shows a band between 3800 and 3000 cm^{-1} , assigned to vibration bands due to the group

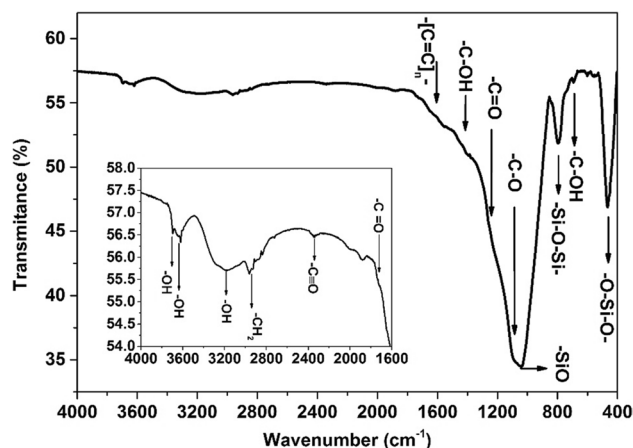


Fig. 4 The FTIR spectra of the SCBA

hydroxyl (OH^-) (Frías et al. 2011; Mor et al. 2019). The presence of three bands in the range of OH-group vibrations was noted in the FT-IR spectrum. A narrow peaks at 3696 and 3640 cm^{-1} can be attributed to OH stretching vibration by hydroxyl groups (Salman et al. 2011a) derived from the regularly distributed group OH^- in the structure. The wide band at 3180 cm^{-1} is related to a randomly placed hydroxyl group in the structure (Kalembkiewicz et al. 2018). Between 2830–2965 cm^{-1} peak showed stretching correspond to asymmetric and symmetric vibrations of $-\text{CH}_2$ group (Ahmad et al. 2018). The peak at 2340 cm^{-1} denotes $\text{C}\equiv\text{C}$ stretching (Salman et al. 2011a). The band corresponding to the carboxylic group $\text{C}=\text{O}$ is observed

as small shoulder at 1720 cm^{-1} , whereas the band due to O–H deformation coupled with C–O stretching vibrations can be observed at 1237 cm^{-1} . The peak at 1060 cm^{-1} indicates the existence of C–O stretching vibrations in alcohols, phenols, acids, ethers, or esters (Trivedi et al. 2016). Silverstein et al. (2005) reported that strong Si–O bands appear at $830\text{--}1110\text{ cm}^{-1}$, which is consistent with 1040 cm^{-1} band found on the FTIR spectra of SCBA. The band at approximately 798 cm^{-1} is attributed to the Si–O–Si symmetric stretching vibration of quartz (Yan et al. 2012). The band at 467 cm^{-1} in the IR spectrum is related to the bending vibrations of SiO_4 tetrahedra, related to the presence of silica glass and quartz (Jovanovski and Makreski 2016). All those intense transmittance bands evidence the large amount of silica on composition of the SCBA.

The TGA/DTG curves of the SCBA are shown in Fig. 5. As noted, there are four main thermal events: at $42.14\text{ }^\circ\text{C}$, $312.38\text{ }^\circ\text{C}$, $534.75\text{ }^\circ\text{C}$ and $916.11\text{ }^\circ\text{C}$. Under air atmosphere, the first and second zones correspond to removal of water moisture and light volatiles up to $423\text{ }^\circ\text{C}$, with a total loss of about 7.6%. Then, there is the active pyrolysis and oxidation zone from $423\text{ }^\circ\text{C}$ to $615\text{ }^\circ\text{C}$ with total degradation of 16.3%. The sample contains carbonaceous matter produced as a consequence of the incomplete combustion of bagasse, in such a way that part of the fibres was decomposed and carbonized in the boilers (Cordeiro et al. 2009). Subsequently, the sample weight remains almost constant with total degradation of 0.4% up to $1000\text{ }^\circ\text{C}$. The residue left at $1000\text{ }^\circ\text{C}$ is about 75.7% of the original sample weight. Therefore, the total mass loss was 24.3%, which is consistent with the loss on ignition analysis (23.6%).

The point of zero charge has traditionally been defined as the pH value at which the surface density of positive charges equals that of negative charges (ie, zero net electric charge); is a characteristic parameter for a given surface of a solid in a given aqueous solution (electrolyte) (Rey et al. 2017; Sposito 1998). Their knowledge is important to predict the

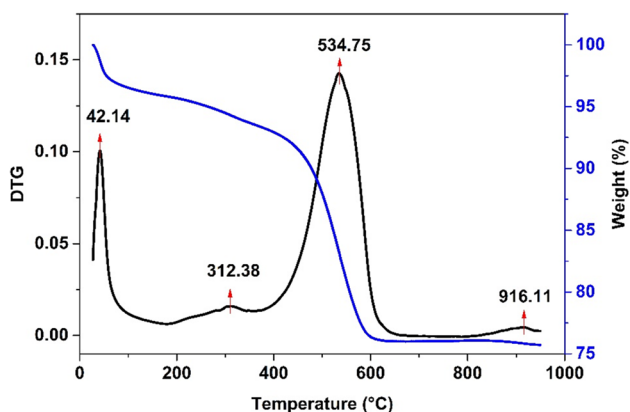


Fig. 5 TGA/DTG curve of SCBA

ionization of surface functional groups and their interaction with species in solution; for pH values lower than pH_{pzc} , the surface charge is positive and the adsorption of anions is favored (Freitas et al. 2015). The graph of initial pH versus ΔpH was obtained (Fig. 6) and the null intersection point corresponded to the zero charge potential. The pH_{pzc} for the adsorbent in this study was 8.45. Anionic dyes have components that cause their molecule dissociate into negatively charged ions in an aqueous solution (Salleh et al. 2011). The Acid Red 27 contain sulfonic groups, present as sodium sulfonates, which give the dye molecules a negative charge, and making the AR27 an anionic dye. At pH values lower than pH_{pzc} , the adsorbent surface charge is positive, favoring the adsorption of anions (Freitas et al. 2015). Since the AR27 dye is anionic, the range to be used in further studies is $\text{pH} < 8.45$.

Adsorption results

Adsorption kinetics and effect of contact time

The adsorption kinetics is an important factor to evaluate the performance of the adsorbent against a certain adsorbate. It describes the rate of adsorbate removal in the fluid medium and the time required for the adsorption to complete. The pseudo-first-order (PFO), pseudo-second-order (PSO), Intraparticle Diffusion and Elovich models were used to fit the time-concentration profile of adsorption of AR27 onto SCBA adsorbent. The models were evaluated using residual sum of squares (RSS), coefficient of determination (R^2) and chi-square factor (χ^2). The kinetic parameters obtained from the models are presented in Table 3.

The kinetic experiment showed that the steady state was reached in 240 min (Fig. 7). The initial slope observed in the

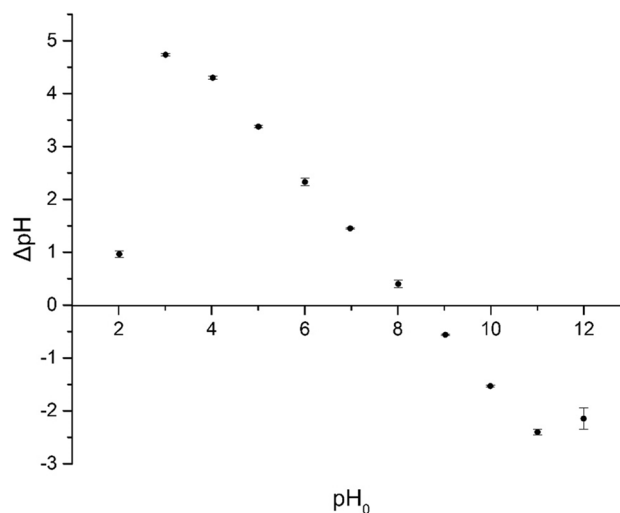


Fig. 6 Determination of pH_{pzc} for SCBA

Table 3 Kinetic parameters for AR27 dye adsorption by SCBA adsorbent and residual sum of squares (RSS) from nonlinear regression analysis

Adsorption kinetics	Parameter	Value
Pseudo-first-order	Predicted q_e ($\text{mg}\cdot\text{g}^{-1}$)	1.8214 ± 0.0553
	k_1 (min^{-1})	0.0203 ± 0.0020
	RSS	0.1159
	R^2	0.9662
	χ^2	0.0116
Pseudo-second-order	Predicted q_e ($\text{mg}\cdot\text{g}^{-1}$)	2.1240 ± 0.0511
	k_2 ($\text{g}\cdot\text{mg}^{-1}\cdot\text{min}^{-1}$)	0.0113 ± 0.0012
	RSS	0.0380
	R^2	0.9889
	χ^2	0.0038
Intraparticle diffusion	k_{id} ($\text{mg}\cdot\text{g}^{-1}\cdot\text{min}^{-1/2}$)	0.0982 ± 0.0097
	C ($\text{mg}\cdot\text{g}^{-1}$)	0.2970 ± 0.1071
	RSS	0.3366
	R^2	0.9018
	χ^2	0.0336
Elovich	α	0.0883 ± 0.0126
	β	2.1005 ± 0.1301
	RSS	0.0582
	R^2	0.9830
	χ^2	0.0058

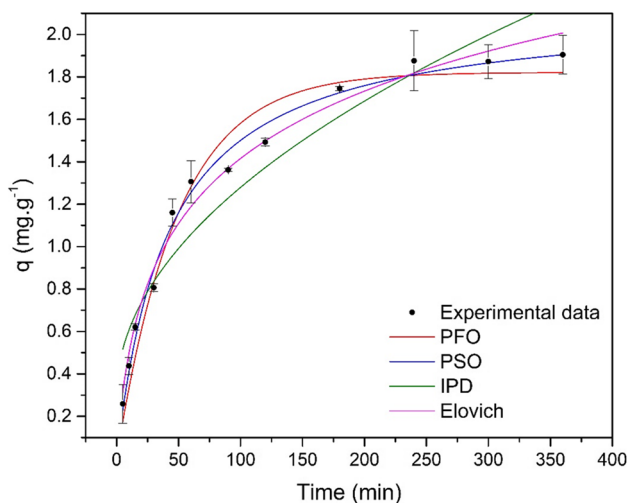


Fig. 7 Kinetic models plots for the removal of AR27 by SCBA

first 200 min of contact reflects rapid initial surface adsorption due to availability of SCBA sorption sites for the AR27 dye, before a period of slow adsorption as available sites decrease and equilibrium is reached after site saturation. The pseudo-second order model best fitted the experimental data, with a coefficient of determination (R^2) equal to 0.989, greater than the others, and a chi-square factor (χ^2)

equal to 0.0038 and RSS equal to 0.03798, smaller than the others. In this model, it is assumed that the rate-limiting step may be surface adsorption, where the removal of the compound from a solution is due to physicochemical interactions between adsorbent and adsorbate (Robati 2013; Ho and McKay 1999).

Effect of solution pH on dye adsorption

The adsorption behavior of the AR27 dye by the SCBA at pH 2 to 12 are shown in Fig. 8. The SCBA had a maximum adsorption of the AR27 dye equal to 77% at $\text{pH}_0 = 2.0$; At $\text{pH}_0 = 3.0$ it dropped to 35.3%. Removal dropped to an average of approximately 29.0%, remaining nearly constant over the pH_0 range of 4 to 9. From this pH value onwards, removal dropped to 2.3% at $\text{pH}_0 = 12$.

Under highly basic conditions, the dye removal efficiency and the adsorption capacity decreased due to the accumulation of negative charge on the adsorbent surface, generating an electrostatic repulsion with the deprotonated dye molecules (sulfonate groups). This repulsive force between the anionic dye molecules and the SCBA surface was mainly responsible for the very low dye removal at high pH.

In a solution with a very acidic pH, it was expected that the removal capacity would decrease if the electrostatic interaction were the only mechanism for dye adsorption (Al-Degs et al. 2008), since the adsorbent would be positively charged and with its carboxylic groups protonated and the dye molecules would be neutral or partially positively charged. At this pH, the sulfonate groups of the dyes would be practically all protonated ($-\text{SO}_3\text{H}$, that is, neutral) and protonation of nitrogen atoms is also likely. Therefore, it is possible that the adsorption of AR27 on SCBA also occurs through hydrogen bonds and ion- π like interaction. The neutral characteristic of the dye salt AR27 focuses on practically

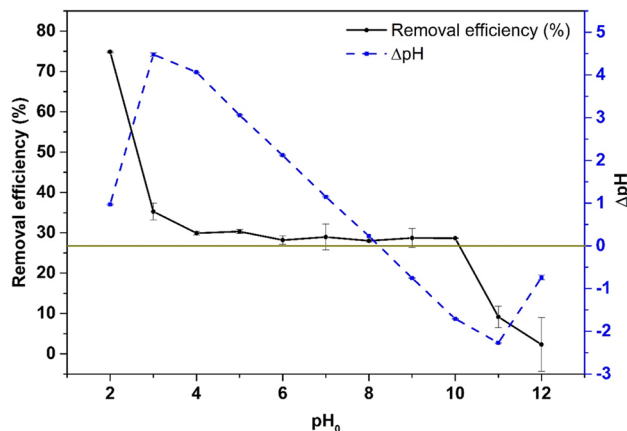


Fig. 8 Effect of solution pH on extent of dye adsorption (Experimental conditions: initial dye concentration $30 \text{ mg}\cdot\text{L}^{-1}$; adsorbent dosage $4 \text{ g}\cdot\text{L}^{-1}$; stirring speed 300 rpm; temperature: $30 \pm 1 \text{ }^\circ\text{C}$)

do not change the pH_{pzc} and the ΔpH curve shape of the SCBA.

Effect of Adsorbent Dosage

From Fig. 9, it is clear that the percentage of dye removal increased as the amount of SCBA was increased, up to a dosage of 6 g.L^{-1} ; thereafter, the removal percentage underwent little change, as the incremental dye removal becomes very low as its concentration on the surface and in the solution reach equilibrium each other. The initial increase in removal efficiency can be attributed to the fact that more surface area is available, with consequent availability of a greater number of active sites, with increasing adsorbent dose. However, continuously increasing the dosage maintains or even may cause a drop in the removal value due to adsorbent particle interactions such as agglomeration, leading to a decrease in the total available surface area of the adsorbent (Mosarca et al. 2020). Indeed, the adsorption capacity of AR27 decreased with increasing adsorbent dosage, a reduction in the adsorption efficiency of the adsorbent per mass unit. Therefore, to weigh the material saving and the adsorption capacity and removal percentage, the optimal adsorbent dosage was selected as 4 g.L^{-1} for subsequent experiments.

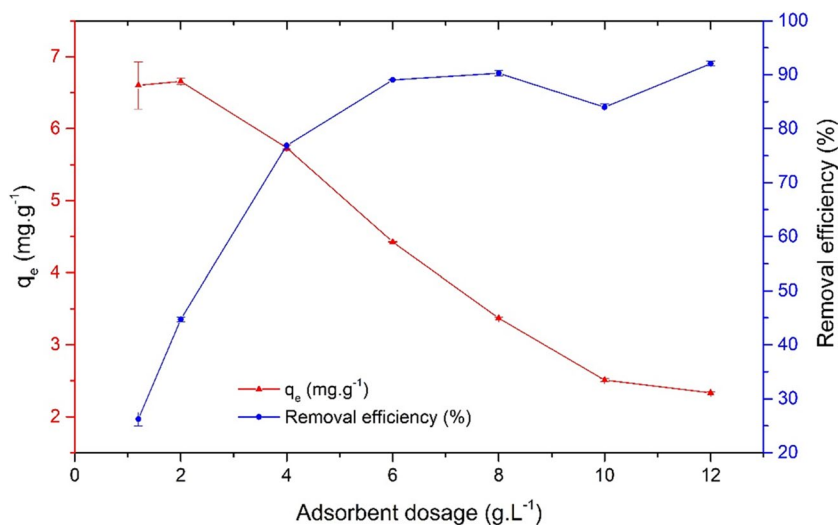
Adsorption isotherm

Linear and nonlinear isotherm models such as Freundlich, Langmuir, Temkin and were used to fit adsorption experimental data, Fig. 10. The residual sum of squares (RSS), coefficient of determination (R^2) and chi-square factor (χ^2) were used to test all models used in this study. The parameters of investigated isotherms obtained from the models are presented in Table 4. The adsorption equilibrium experiments showed that the experimental adsorptive

capacity reaches 10.20 mg.g^{-1} . It is observed that the Freundlich model was the one that best adjusted to the equilibrium data. The Freundlich isotherm is convenient when intending to describe a non-ideal and reversible adsorptive system, on heterogeneous surfaces (adsorbent surface sites have a spectrum of different binding energies), not restricted to monolayer formation, and can be applied to multilayer adsorption (Ayawei et al. 2017; Pezoti et al. 2016). This result corroborates the fact that ash comes from sugarcane bagasse, which has a heterogeneous microstructure and an extremely turbulent burning process.

Table 5 lists a comparison of maximum monolayer adsorption capacity of dye AR27 with various adsorbents and some dyes with the bagasse ash as adsorbent. From this table, it is important to highlight that depending on the adsorbent-adsorbate interactions and the surface area available for adsorption, the q_{max} for a certain adsorbent can vary considerably. As expected, activated carbon presents the best adsorption results for the different adsorbates presented, except for the adsorption of Basic green 4 on commercial activated carbon. For sugarcane ash, the value found here is consistent with other works, presenting a maximum value of 15.01 mg.g^{-1} , one order of magnitude. Above that we have the adsorption of basic green 4 and methylene blue, with two orders of magnitude for ash. Despite its low adsorptive capacity for Acid Red 27 is important to consider that bagasse ash is an industrial tailing, would be acquired for free and used without pretreatment. In the search for an environmentally friendly economy this lower environmental impact issue is of most importance. Nevertheless, a more detailed study is needed to quantify the real impact for the environment and economy with the application of SCBA for water and effluents treatments.

Fig. 9 Effect of adsorbent dosage on the adsorption of dye AR27 by SCBA (Experimental conditions: initial dye concentration 30 mg.L^{-1} ; $\text{pH}_0 = 2.0$; stirring speed 300 rpm; temperature = $30 \pm 1 \text{ }^\circ\text{C}$, $t = 4 \text{ h}$)



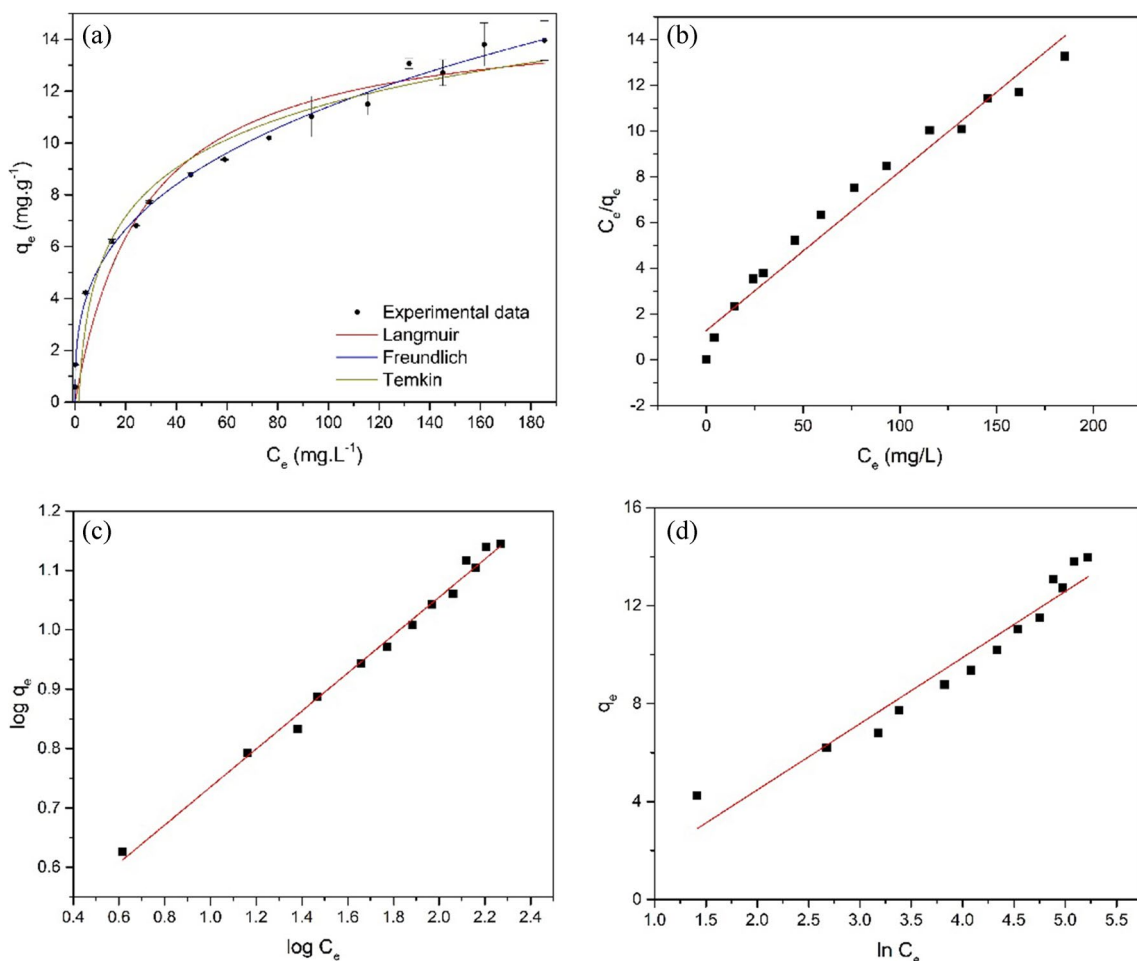


Fig. 10 Equilibrium isotherms for the adsorption of AR27 by SCBA: (a) Lagmuir, Freundlich and Temkin non-linearized; (b) Lagmuir linearized; (c) Freundlich linearized; (d) Temkin linearized (Experimen-

tal conditions: adsorbent dosage=4 g.L⁻¹; mixing rate=300 rpm; T=30±1 °C; initial conc.: 2.5—240 mg.L⁻¹; contact time=4 h)

Table 4 Coefficients obtained for sorption isotherm models for AR27 dye adsorption by SCBA and RSS, R² and χ² from linear and nonlinear regression analysis (Experimental conditions: adsorbent dosage=4 g.L⁻¹; mixing rate=300 rpm; T=30±1 °C; initial conc.: 2.5—240 mg.L⁻¹; contact time=4 h)

Isotherm model	Parameter	Linear	Nonlinear
<i>Langmuir</i>	q _{max} (mg.g ⁻¹)	14.3781 ± 0.7318	15.0083 ± 0.8738
	K _L (L.mg ⁻¹)	0.0545 ± 0.0145	0.03675 ± 0.0080
	RSS	9.0355	13.4012
	R ²	0.9649	0.9432
	χ ²		1.0309
<i>Freundlich</i>	K _F ((mg.g ⁻¹).(mg.L ⁻¹) ^{-1/n})	2.6029 ± 0.0899	2.4595 ± 0.2216
	n	3.1268 ± 0.0810	3.0029 ± 0.1779
	RSS	0.0021	3.5165
	R ²	0.9920	0.9851
	χ ²		0.2705
<i>Temkin</i>	K _T (L.mg ⁻¹)	0.7098 ± 0.5926	0.7098 ± 0.2178
	B = $\frac{RT}{b}$	2.7014 ± 0.2003	2.7014 ± 0.2156
	RSS	6.5676	8.9913
	R ²	0.9378	0.9619
	χ ²		0.6916

Table 5 Comparison of the maximum monolayer adsorption of dyes onto adsorbents

Adsorbent	Preparation	Dye	q_{\max} (mg.g ⁻¹)	Ref
Sugarcane bagasse ash	Residue of burning in high pressure boiler	Acid Red 27	15.01	This work
Activated Carbon Web Prepared from Acrylic Fibrous Waste	Physical activation under the layer of charcoal in high temperature furnace (800–1200 °C)	Acid Red 27	21.68	Salman-Naeem et al. 2018
Chitosan-polyethyleneimine beads	Graft copolymerization under microwave irradiation	Acid Red 27	48.30	Yusof et al. 2020
Activated Carbon Prepared from Coconut Husk Fiber	Activation with ZnCl ₂ at high temperature	Acid Red 27	333.33	Al-Aoh et al. 2013
Commercial Activated Carbon	Commercial product	Acid Red 27	166.67	Al-Aoh et al. 2013
γ -Fe ₂ O ₃ nanoadsorbents	Commercial product	Acid Red 27	16.32	Nassar 2010
Polypyrrole/SrFe ₁₂ O ₁₉ /graphene oxide nanocomposite	The SrFe ₁₂ O ₁₉ (SrM) nanoparticles were synthesized by citrate sol-gel process. The GO particles were synthesized by Hummers' method. The PPY/SrM/GO nanocomposite powder was fabricated through in situ polymerization	Acid Red 27	294.11	Ebrahimpoor et al. 2019
Bagasse fly ash	Residue of burning in high pressure boiler	Basic green 4	116.28	Mane et al. 2007
Bagasse fly ash	Residue of burning in high pressure boiler	Basic Green 4	170.33	Mall et al. 2005
Activated carbons commercial grade	Commercial product		8.27	
Activated carbons laboratory grade	Commercial product		42.18	
Bagasse fly ash	Residue of burning in high pressure boiler	Acid Orange 10	18.80	Mall et al. 2006
		Basic violet 1	26.25	
Bagasse fly ash	Residue of burning in high pressure boiler	Methylene blue	64.61	Gupta et al. 2000

Adsorption thermodynamics and effect of temperature

Adsorption thermodynamic parameters were derived from the linear form of the van't Hoff equation and the thermodynamic definition of chemical equilibrium (Lima et al. 2020), depicted in the Eqs. 3 and 4, respectively.

$$\ln b = \frac{\Delta S^\circ}{R} - \frac{\Delta H^\circ}{RT} \quad (3)$$

$$\Delta G^\circ = -RT \ln b \quad (4)$$

where ΔG° is the change in the Gibbs free energy (kJ.mol⁻¹); ΔH° is the change in enthalpy (kJ.mol⁻¹), and ΔS° is the change in entropy (J.mol⁻¹.K⁻¹), R is the gas constant (8.314 J.mol⁻¹.K⁻¹), T is the thermodynamic temperature (K). The adsorption equilibrium constant (b) was derived from the isotherm data at different temperatures using the Langmuir and Temkin nonlinear models (K_L and K_T , expressed in L.mg⁻¹). The equilibrium constants K_L and K_T must become dimensionless for use in the Vant' Hoff equation; for this purpose, Eq. 5 was used (Lima et al. 2019).

$$b = K_{\text{ads}}^\circ = \frac{(1000 \cdot \text{K} \cdot \text{molecular weight of adsorbate}) \cdot [\text{Adsorbate}]^\circ}{\gamma} \quad (5)$$

where γ is the coefficient of activity (dimensionless, it is considered that the adsorbate solution is very diluted to consider that its value is unitary), $[\text{Adsorbate}]^\circ$ is the standard concentration of the adsorbate (1 mol.L⁻¹), K is the and K_{ads}° is the thermodynamic equilibrium constant that is dimensionless.

The parameters of the investigated isotherms obtained by the linear and nonlinear Langmuir, Freundlich, Temkin models are presented in Table S3 for the three temperatures. It can be seen that for these temperatures the model that best fits the experimental data were also the Freundlich models. Furthermore, we have added the BET type II isotherm model to proceed the thermodynamic calculation with better fitted data, as Freundlich parameters does not have thermodynamic correlation to Vant' Hoff equation. The parameters of BET isotherm model are listed in Table S4. The BET model is an extension of Langmuir's theory and considers that adsorption can occur

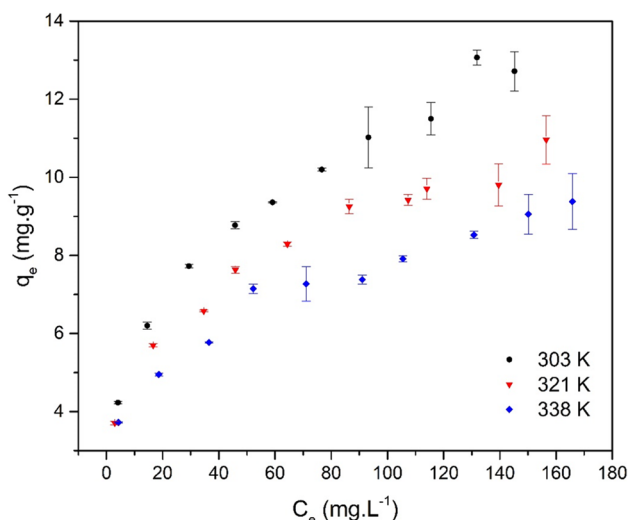


Fig. 11 Effect of temperature on AR27 adsorption performance by SCBA (Experimental conditions: adsorbent dosage=4 g.L⁻¹; mixing rate=300 rpm; T=30±1 °C; initial conc.: 2.5–240 mg.L⁻¹; contact time=4 h)

Table 6 Thermodynamic parameters for adsorption of AR27 onto SCBA

Adsorption modeling		Temperature (K)		
		303	321	338
Langmuir	ΔG°_{ads} (kJ.mol ⁻¹)	-33.47	-35.46	-37.34
	ΔH°_{ads} (kJ.mol ⁻¹)	7.33		
	ΔS°_{ads} (J.mol ⁻¹ .K ⁻¹)	110.49		
Temkin	ΔG°_{ads} (kJ.mol ⁻¹)	-48.20	-51.07	-53.77
	ΔH°_{ads} (kJ.mol ⁻¹)	14.48		
	ΔS°_{ads} (J.mol ⁻¹ .K ⁻¹)	159.14		
BET	ΔG°_{ads} (kJ.mol ⁻¹)	-10.25	-11.49	-12.71
	ΔH°_{ads} (kJ.mol ⁻¹)	11.47		
	ΔS°_{ads} (J.mol ⁻¹ .K ⁻¹)	71.53		

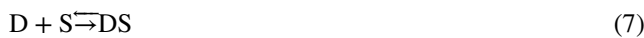
through multiple layers of adsorbate on the surface of the adsorbent. A non-linear version of this model, the BET type II isotherm is used to describe adsorptive processes in the liquid phase, and its mathematical model is given by Equation S11 in Table S2. For the BET model, the equilibrium constant is at dimensionless form, and can be applied directly to the Vant' Hoff equation.

Figure 11 shows the adsorption isotherms for AR27 dye on SCBA at three different temperatures. Table 6 shows the values of the thermodynamic parameters ΔG°_{ads} , ΔH°_{ads} , ΔS°_{ads} for the adsorption of AR27, using the K_L (Langmuir) K_T (Temkin) and K_B (BET) constants obtained from the isotherms at temperatures of 303, 321 and 338 K. In Fig. S3 we can observe the graph of $\ln b$ versus T^{-1} (K⁻¹) used in the determination of thermodynamic parameters.

The magnitude of the enthalpy (less than 40 kJ.mol⁻¹) suggests that the adsorption process occurs through a physisorption (physical process), since it does not assume sufficient values to indicate ruptures and formation of chemical bonds. The low values of the enthalpy evidence that the interaction between AR27 dye and the SCBA may be weak, as there is a tendency that as greater the energy involved as greater the propensity for formation of chemical bonds between adsorbent-adsorbate (Sahmoune 2018).

The negative ΔG°_{ads} and positive ΔS°_{ads} confirm a spontaneous adsorption process and suggests affinity of the SCBA for AR27 dye, with an increase in spontaneity as temperature increases from 303 to 338 K. The endothermic value obtained for ΔH°_{ads} appears to be inconsistent with the decrease of adsorption as the increase of the temperature. Some apparently inconsistent data have been founded in literature, suggesting an endothermic process, however the maximum capacity of adsorption decrease with the temperature increasing (Al-Aoh et al. 2013; Salman et al. 2011b, 2011a; Alver and Metin 2012; Mittal 2006). This behavior have been linked to the isosteric enthalpy, in analogy to the physisorption of gases but not described in depth (Mane et al. 2007). As expected for a physisorption process, the increase of the temperature enhance the distribution of dye molecule with energy higher than the electrostatic potential, which reflect at the decrease of the dye adsorption (Nuhnen and Janiak 2020).

In this way, its suggest need to understand the physisorption in aqueous environment as a combination of two main processes, the desorption of water ΔH°_W and the adsorption of the dye ΔH°_D at the ash surface. Thus, the constant of the equilibrium determined by the isothermal modeling need to involve the contribution of both processes, as follow Eqs. 6–8, where: W is the water; S is the substrate; and D is the dye.



$$b = b_w \cdot b_{dye} = \frac{[W][S]}{[WS]} \cdot \frac{[DS]}{[D][S]} \tag{8}$$

Above consideration implies the ΔH°_{ads} of Van't Hoff be a contribution of $\Delta H^{\circ}_{Wdes} + \Delta H^{\circ}_{Dads}$. Although, this enthalpy consider only the energy involved in the equilibrium of the reaction. However in analogy of gas physisorption its possible to involve the isosteric enthalpy of the adsorption (as a condensation like process) of the dye, $\Delta H_D(q_e)$, onto the SCBA surface. Therefore, for a dye physisorption the $\Delta H_D(q_e)$ assumed can be calculated using the adapted Clausius-Clapeyron approach, Eq. 9, for $P = RTC_e$. The slope m of the straight line with the three data points at $\ln(T_1 C_{e1})|1/T_1$,

$\ln(T_2 C_{e2})/T_2$ and $\ln(T_3 C_{e3})/T_3$ at equal loading q_e will give $\Delta H_D(q_e)$ according to Eq. 10 (Nuhnen and Janiak 2020).

$$\frac{d(RTC_e)}{dT} = \frac{C_e \cdot \Delta H_D(q_e)}{-T} \quad (9)$$

$$\Delta H_D(q_e) = m \cdot R \quad (10)$$

A last consideration can be made for the “first few molecules” adsorbed ($q_e \rightarrow 0$) (Nuhnen and Janiak 2020). In this stage, the ΔV of the “dye condensation” onto surface of the adsorbent tend to zero ($\Delta V \rightarrow 0$) and is reasonable to consider that $\Delta H_{Dads}^0 \approx \Delta H_D(q_e \rightarrow 0) = \Delta H_D^0$. In conclusion, when $\Delta H_{Dads}^0 < 0$, the seeming discussed inconsistency happens for $|\Delta H_{Dads}^0| < |\Delta H_{Wdes}^0|$, resulting in a positive value of the ΔH_{ads}^0 in the Vant' Hoff equation; also for $\Delta H_{Dads}^0 > 0$.

Additionally, the ΔH_D^0 value can differ distinctly from ΔH_D for the bulk adsorption. For the AR27 adsorption onto SCBA, the approach of the $\Delta H_D(q_e)$ values based on Freundlich model gives the values of $\Delta H_D^0 = 9.2 \text{ kJ.mol}^{-1}$, described in Supplementary Information (S4). Considering the value of the $\Delta H_{ads}^0 = 11.5 \text{ kJ.mol}^{-1}$ obtained from BET approaches, the value for the ΔH_{Wdes}^0 was 2.3 kJ.mol^{-1} . $\Delta H_{ads}(q_e) = \Delta H_{Wdes}^0 + \Delta H_D(q_e)$ was plotted in Fig. S11, considering the ΔH_{Wdes}^0 as a constant.

Applying this same procedure for the others apparently inconsistent values of the ΔH_{ads}^0 enthalpy available in literature, Table S5, the values of ΔH_{Wdes}^0 calculated were between 3.5 and 31.0 kJ.mol^{-1} . Despite some adsorbents initially presented an endothermic behavior, analyzing the Fig. S5 to S10 was clear that increasing the dye adsorbed amount the isosteric enthalpy changes reaching to be an exothermic behavior which explain the unfavorable adsorption with the increase of the temperature to high adsorbed amount.

Influence of coexisting anions

Coexisting anions such as chloride, sulfate and bicarbonate are typically present in effluents. These anions can compete with the adsorbate and interfere in the removal efficiency. As a result, the effects of these coexisting anions on the AR27 adsorption are shown in Fig. 12.

The presence of chloride anions proved to have little effect on the removal efficiency of AR27, as the removal decreased from 66.8% to 63.6%. On the other hand, the effects of sulfate and bicarbonate anions on the removal of AR27 were significant. In the presence of sulfate at 0.1 M, the removal efficiency of AR27 decreased to 43.5%, while at a concentration of 0.1 M of bicarbonate, the removal of AR27 decreased to 28.2%. In other words, sulfate and bicarbonate compete more with AR27 for active sites in the SCBA than does the chloride anion. In the concomitant

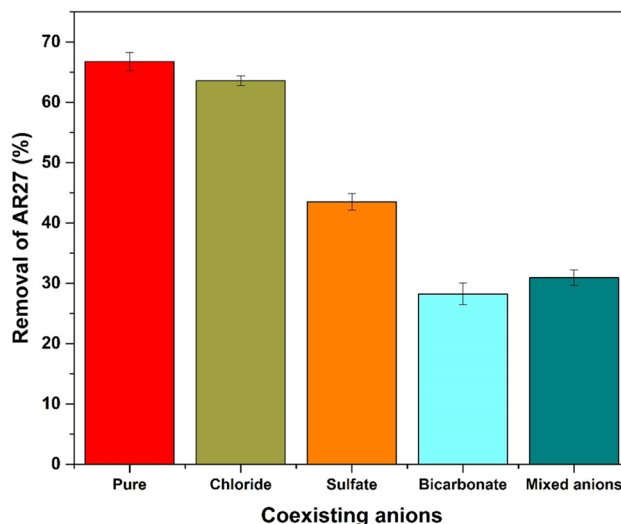


Fig. 12 Effect of coexisting anions on AR27 removal at fixed initial concentration of AR27 = 30 mg.L^{-1} , coexisting anion concentration = 0.1 M , adsorbent dose = 4 g.L^{-1} , shaking rate = 300 rpm , contact time = 4 h , $\text{pH} = 2$, $T = 30 \pm 1 \text{ }^\circ\text{C}$

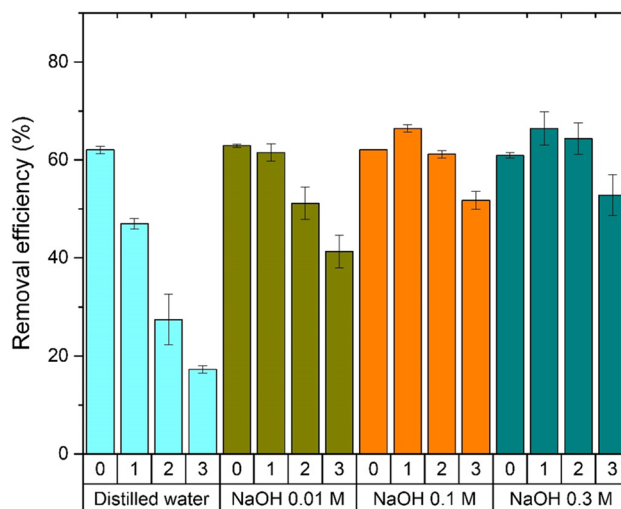


Fig. 13 Batch adsorption/desorption cycles after regeneration with NaOH (Experimental conditions: initial concentration of AR27 = 30 mg.L^{-1} , adsorbent dose = 4 g.L^{-1} , shaking rate = 300 rpm , contact time = 4 h , $\text{pH} = 2$, $T = 30 \pm 1 \text{ }^\circ\text{C}$)

presence of the mentioned anions (0.1 M of each), the removal fell to 30.9%.

Regeneration and reuse of SCBA

Three SCBA adsorption-regeneration cycles were performed as shown in Fig. 13. For regeneration with distilled water, the adsorbent lost around 70% of its removal efficiency after three consecutive cycles of adsorption–desorption

experiments. For regeneration with 0.01 M NaOH, the efficiency of the first cycle remained at the same level as the original cycle, but decreased by 35% after the next two cycles. For regeneration with 0.1 and 0.3 M NaOH, the removal efficiency increased slightly after the first cycle, decreasing in the next two, but managing to maintain > 50% removal after the third cycle.

Therefore, SCBA has great potential for use in the treatment of effluents containing AR27 dye, because it can be reused through simple regeneration, and combined with its ability to maintain removal efficiency after two cycles, it becomes even more economical and sustainable.

Conclusions

The present study shows that sugarcane bagasse ash, a residue obtained from the sugar mill, can be used as an adsorbent for the removal of Acid Red 27 dye in aqueous solution. The kinetics study showed that equilibrium was reached in 4 h, with the adsorption kinetics best represented by the pseudo-second order model. The pH influence to the adsorptive equilibrium showed that the maximum adsorption of the dye by the ash occurred at pH_0 equal to 2.0. For the equilibrium study, the results showed that the Freundlich isotherm described well the adsorption behavior of the dye in the studied concentration ranges, with adsorption capacity of $14 \text{ mg}\cdot\text{g}^{-1}$ to the most concentrated solution studied at optimal pH_0 ; the maximum adsorption capacity of Langmuir was $15 \text{ mg}\cdot\text{g}^{-1}$. The thermodynamic adsorption parameters evaluated by Vant' Hoff equation with fitted parameter for Langmuir, Temkin and BET demonstrate an endothermic, spontaneous and indicate a physisorption mechanism, with $\Delta H_{\text{ads}}^{\circ} < 15 \text{ kJ}\cdot\text{mol}^{-1}$. Clausius-Clapeyron approach adapted for adsorption in liquid environment was successfully applied to determine the isosteric enthalpy behavior of Acid Red 27 at sugarcane bagasse ash, which the $\Delta H_{\text{D}}^{\circ} = 9.2 \text{ kJ}\cdot\text{mol}^{-1}$ was founded. However, ΔH_{D} for the bulk adsorption is exothermic reaching absolute values higher than $25 \text{ kJ}\cdot\text{mol}^{-1}$. The effect of coexisting anions were studied for the presence of chloride, sulfate and bicarbonate. The results showed small interference of chloride but high influence of bicarbonate, with adsorption capacity reaching reduction of almost 60%. Regeneration of SCBA with sodium hydroxide was able to preserve its initial removal capacity for two cycles. Sugarcane bagasse ash seems to have potential to be used as a cheap adsorbent in the removal of Acid Red 27 dye in low concentrated solutions.

Supplementary Information The online version contains supplementary material available at <https://doi.org/10.1007/s11356-024-31917-x>.

Acknowledgements We thank CNPq, CAPES, and FACEPE (all from Brazil) for their financial support. We are also grateful to the Petribu

S.A. sugarcane mill (Lagoa de Itaenga, Brazil) and the VitaSense LTDA for kindly providing the sugarcane bagasse ash and sample of the dye, respectively.

Author contributions All authors contributed to the study conception and design. Material preparation, data collection and analysis were performed by Joana Eliza de Santana, Fábio Gabriel Silva de Andrade and Aldebarã Fausto Ferreira. The review, supervision and project administration were performed by Marcos Gomes Ghislandi and Maurício Alves da Motta Sobrinho. The first draft of the manuscript was written by Joana Eliza de Santana and all authors commented on previous versions of the manuscript. All authors read and approved the final manuscript.

Funding This work was supported by Conselho Nacional de Desenvolvimento Científico e Tecnológico – CNPq (Grant number 142446/2018–1) and Fundação de Amparo à Ciência e Tecnologia do Estado de Pernambuco – FACEPE (BIC-0358–3.07/23).

Data Availability The authors declare that the data supporting the findings of this study are available within the paper and its Supplementary Information files. Should any raw data files be needed in another format they are available from the corresponding author upon reasonable request.

Declarations

Ethical approval Not applicable.

Consent to participate Not applicable.

Consent to publish Not applicable.

Competing interests The authors have no relevant financial or non-financial interests to disclose.

References

- Ahmad S, Wong YC, Veloo KV (2018) Sugarcane bagasse powder as biosorbent for reactive red 120 removals from aqueous solution. In IOP Conf Ser: Earth Environ Sci 140:012027. <https://doi.org/10.1088/1755-1315/140/1/012027>
- Al-Aoh HA, Maah MJ, Yahya R, Abas MRB (2013) A comparative investigation on adsorption performances of activated carbon prepared from coconut husk fiber and commercial activated carbon for acid red 27 dye. Asian J Chem 25:9582. <https://doi.org/10.14233/ajchem.2013.15082A>
- Al-Degs YS, El-Barghouthi MI, El-Sheikh AH, Walker GM (2008) Effect of solution pH, ionic strength, and temperature on adsorption behavior of reactive dyes on activated carbon. Dyes Pigm 77:16–23. <https://doi.org/10.1016/j.dyepig.2007.03.001>
- Alver E, Metin AU (2012) Anionic dye removal from aqueous solutions using modified zeolite: Adsorption kinetics and isotherm studies. Chem Eng J 200–202:59–67. <https://doi.org/10.1016/j.cej.2012.06.038>
- Andrade Neto JDS, de França MJS, de Amorim Junior NS, Ribeiro DV (2021) Effects of adding sugarcane bagasse ash on the properties and durability of concrete. Constr Build Mater 266:120959. <https://doi.org/10.1016/j.conbuildmat.2020.120959>
- Arabkhani P, Javadian H, Asfaram A, Sadeghfard F, Sadegh F (2021) Synthesis of magnetic tungsten disulfide/carbon nanotubes nanocomposite (WS₂/Fe₃O₄/CNTs-NC) for highly efficient ultrasound-assisted rapid removal of amaranth and brilliant blue FCF

- hazardous dyes. *J Hazard Mater* 420:126644. <https://doi.org/10.1016/j.jhazmat.2021.126644>
- Ayawei N, Ebelegi AN, Wankasi D (2017) Modelling and interpretation of adsorption isotherms. *J Chem* 2017:1–11. <https://doi.org/10.1155/2017/3039817>
- Chhabra M, Mishra S, Sreerishnan TR (2015) Immobilized laccase mediated dye decolorization and transformation pathway of azo dye acid red 27. *J Environ Health Sci Eng* 13:1–9. <https://doi.org/10.1186/s40201-015-0192-0>
- CONAB - Companhia Nacional de Abastecimento (2023a) Série Histórica das Safras. <https://www.conab.gov.br/info-agro/safras/serie-historica-das-safras> (in Portuguese). Accessed 28 July 2023
- CONAB - Companhia Nacional de Abastecimento (2023b) Análise mensal da cana-de-açúcar (maio/junho 2023). <https://www.conab.gov.br/info-agro/analises-do-mercado-agropecuário-e-extrativista/analises-do-mercado/historico-mensal-de-cana-de-acucar> (in Portuguese). Accessed 28 July 2023
- Cordeiro GC, Toledo Filho RD, Fairbairn EDMR (2009) Characterization of sugar cane bagasse ash for use as pozzolan in cementitious materials. *Quim Nova* 32:82–86. <https://doi.org/10.1590/S0100-40422009000100016>
- Deng Z, Sun S, Li H, Pan D, Patil RR, Guo Z, Seok I (2021) Modification of coconut shell-based activated carbon and purification of wastewater. *Adv Compos Hybrid Mater* 4:65–73. <https://doi.org/10.1007/s42114-021-00205-4>
- Ebrahimpoor S, Kiarostami V, Khosravi M, Davallo M, Ghaedi A (2019) Bees metaheuristic algorithm with the aid of artificial neural networks for optimization of acid red 27 dye adsorption onto novel polypyrrole/SrFe₁₂O₁₉/graphene oxide nanocomposite. *Polym Bull* 76:6529–6553. <https://doi.org/10.1007/s00289-019-02700-7>
- FAOSTAT - Food and Agriculture Organization of the United Nations (2023) Countries by commodity. https://www.fao.org/faostat/en/#rankings/countries_by_commodity. Accessed 28 July 2023
- Freitas FBA, Câmara MYF, Freire MDF (2015) Determinação do PCZ de adsorventes naturais utilizados na remoção de contaminantes em soluções aquosas. *Blucher Chem Proc* 3:610–618. <https://doi.org/10.5151/chenpro-5erq-am1>
- Friás M, Villar E, Savastano H (2011) Brazilian sugar cane bagasse ashes from the cogeneration industry as active pozzolans for cement manufacture. *Cement Concr Compos* 33:490–496. <https://doi.org/10.1016/j.cemconcomp.2011.02.003>
- Gan YX (2021) Activated Carbon from Biomass Sustainable Sources. *J Carbon Res* 7:39. <https://doi.org/10.3390/c7020039>
- Gar PS, Suresh N, Bindiganavile V (2017) Sugar cane bagasse ash as a pozzolanic admixture in concrete for resistance to sustained elevated temperatures. *Constr Build Mater* 153:929–936. <https://doi.org/10.1016/j.conbuildmat.2017.07.107>
- Gupta VK, Mohan D, Sharma S, Sharma M (2000) Removal of Basic Dyes (Rhodamine B and Methylene Blue) from Aqueous Solutions Using Bagasse Fly Ash. *Sep Sci Technol* 35:2097–2113. <https://doi.org/10.1081/SS-100102091>
- Ho YS, McKay G (1999) Pseudo-second order model for sorption processes. *Process Biochem* 34:451–465. [https://doi.org/10.1016/S0032-9592\(98\)00112-5](https://doi.org/10.1016/S0032-9592(98)00112-5)
- Jovanovski G, Makreski P (2016) Minerals from Macedonia. XXX. Complementary use of vibrational spectroscopy and X-ray powder diffraction for spectra-structural study of some cyclo-, phyllo- and tectosilicate minerals: A review. *Maced J Chem Chem Eng* 35:125–155. <https://doi.org/10.20450/mjce.2016.1047>
- Kalembkiewicz J, Galas D, Sitarz-Palczak E (2018) The Physicochemical Properties and Composition of Biomass Ash and Evaluating Directions of its Applications. *Pol J Environ Stud* 27:2593–2603. <https://doi.org/10.15244/pjoes/80870>
- Lima EC, Hosseini-Bandegharai A, Moreno-Piraján JC, Anastopoulos I (2019) A critical review of the estimation of the thermodynamic parameters on adsorption equilibria. Wrong use of equilibrium constant in the Van't Hoff equation for calculation of thermodynamic parameters of adsorption. *J Mol Liq* 273:425–434. <https://doi.org/10.1016/j.molliq.2018.10.048>
- Lima EC, Gomes AA, Tran HN (2020) Comparison of the nonlinear and linear forms of the van't Hoff equation for calculation of adsorption thermodynamic parameters (ΔS° and ΔH°). *J Mol Liq* 311:113315. <https://doi.org/10.1016/j.molliq.2020.113315>
- Mahmood T, Saddique MT, Naeem A, Westerhoff P, Mustafa S, Alum A (2011) Comparison of different methods for the point of zero charge determination of NiO. *Ind Eng Chem Res* 50:10017–10023. <https://doi.org/10.1021/ie200271d>
- Mall ID, Srivastava VC, Agarwal NK, Mishra IM (2005) Adsorptive removal of malachite green dye from aqueous solution by bagasse fly ash and activated carbon-kinetic study and equilibrium isotherm analyses. *Colloids Surf, A* 264:17–28. <https://doi.org/10.1016/j.colsurfa.2005.03.027>
- Mall ID, Srivastava VC, Agarwal NK (2006) Removal of Orange-G and Methyl Violet dyes by adsorption onto bagasse fly ash—kinetic study and equilibrium isotherm analyses. *Dyes Pigm* 69:210–223. <https://doi.org/10.1016/j.dyepig.2005.03.013>
- Mane VS, Mall ID, Srivastava VC (2007) Use of bagasse fly ash as an adsorbent for the removal of brilliant green dye from aqueous solution. *Dyes Pigm* 73:269–278. <https://doi.org/10.1016/j.dyepig.2005.12.006>
- Matos WEC, da Silva HDJB, da Paz GM, dos Santos VB (2021) Utilization of sugarcane bagasse ashes as filler or pozzolanic material for the cementitious mortar production: a review. *Materia-Rio De Janeiro* 26. <https://doi.org/10.1590/S1517-707620210004.1322>
- Metivier-Pignon H, Faur C, Le Cloirec P (2007) Adsorption of dyes onto activated carbon cloth: Using QSPRs as tools to approach adsorption mechanisms. *Chemosphere* 66:887–893. <https://doi.org/10.1016/j.chemosphere.2006.06.032>
- Mittal A (2006) Use of hen feathers as potential adsorbent for the removal of a hazardous dye, Brilliant Blue FCF, from wastewater. *J Hazard Mater* 128:233–239. <https://doi.org/10.1016/j.jhazmat.2005.08.043>
- Mor S, Negi P, Ravindra K (2019) Potential of agro-waste sugarcane bagasse ash for the removal of ammoniacal nitrogen from landfill leachate. *Environ Sci Pollut Res* 26:24516–24531. <https://doi.org/10.1007/s11356-019-05563-7>
- Mosoarca G, Vancea C, Popa S, Gheju M, Boran S (2020) Syringa vulgaris leaves powder a novel low-cost adsorbent for methylene blue removal: Isotherms, kinetics, thermodynamic and optimization by Taguchi method. *Sci Rep* 10:17676. <https://doi.org/10.1038/s41598-020-74819-x>
- Nassar NN (2010) Kinetics, mechanistic, equilibrium, and thermodynamic studies on the adsorption of acid red dye from wastewater by γ -Fe₂O₃ nano-adsorbents. *Sep Sci Technol* 45:1092–1103. <https://doi.org/10.1080/01496391003696921>
- Nuhn A, Janiak C (2020) A practical guide to calculate the isosteric heat/enthalpy of adsorption via adsorption isotherms in metal-organic frameworks. *Mof Dalton Trans* 49:10295. <https://doi.org/10.1039/d0dt01784a>
- Patel H (2020) Environmental valorisation of bagasse fly ash: a review. *RSC Adv* 10:31611–31621. <https://doi.org/10.1039/D0RA06422J>
- Patel H (2021) Review on solvent desorption study from exhausted adsorbent. *J Saudi Chem Soc* 25:101302. <https://doi.org/10.1016/j.jscs.2021.101302>
- Patil C, Manjunath M, Hosamane S, Bandekar S, Athani R (2021) Pozzolonic activity and strength activity index of bagasse ash and fly ash blended cement mortar. *Mater Today: Proceedings* 42:1456–1461. <https://doi.org/10.1016/j.matpr.2021.01.251>
- Pezoti O, Cazetta AL, Bedin KC, Souza LS, Martins AC, Silva TL, Santos Júnios OO, Visentainer JV, Almeida VC (2016) NaOH-activated carbon of high surface area produced from guava seeds

- as a high-efficiency adsorbent for amoxicillin removal: Kinetic, isotherm and thermodynamic studies. *Chem Eng J* 288:778–788. <https://doi.org/10.1016/j.cej.2015.12.042>
- Pinedo-Hernández S, Díaz-Nava C, Solache-Ríos M (2012) Sorption behavior of Brilliant Blue FCF by a Fe-Zeolitic tuff. *Water Air Soil Pollut* 223:467–475. <https://doi.org/10.1007/s11270-011-0877-7>
- Rahman NA, Widhiana I, Juliastuti SR, Setyawan H (2015) Synthesis of mesoporous silica with controlled pore structure from bagasse ash as a silica source. *Colloids Surf, A* 476:1–7. <https://doi.org/10.1016/j.colsurfa.2015.03.018>
- Rey C, Combes C, Drouet C, Grossin D, Bertrand G, Soulié J (2017) 1.11 Bioactive Calcium Phosphate Compounds: Physical Chemistry. *Compr Biomater II*:244–290. <https://doi.org/10.1016/B978-0-12-803581-8.10171-7>
- Ribeiro DV, Morelli MR (2014) Effect of calcination temperature on the pozzolanic activity of Brazilian sugar cane bagasse ash (SCBA). *Mater Res* 17:974–981. <https://doi.org/10.1590/S1516-14392014005000093>
- Robati D (2013) Pseudo-second-order kinetic equations for modeling adsorption systems for removal of lead ions using multi-walled carbon nanotube. *J Nanostructure Chem* 3:1–6. <https://doi.org/10.1186/2193-8865-3-55>
- Rouquerol J, Avnir D, Fairbridge CW, Everett DH, Haynes JM, Pernicone N, Ramsay JDF, Sing KSW, Unger KK (1994) Recommendations for the characterization of porous solids (Technical Report). *Pure Appl Chem* 66:1739–1758. <https://doi.org/10.1351/pac199466081739>
- Sahmoune MN (2018) Thermodynamic Properties of Heavy Metals Ions Adsorption by Green Adsorbents. *Green Adsorb Pollut Remov* 193–213. https://doi.org/10.1007/978-3-319-92111-2_6
- Salleh MAM, Mahmoud DK, Karim WAWA, Idris A (2011) Cationic and anionic dye adsorption by agricultural solid wastes: A comprehensive review. *Desalination* 280:1–12. <https://doi.org/10.1016/j.desal.2011.07.019>
- Salman JM, Njoku VO, Hameed BH (2011a) Adsorption of pesticides from aqueous solution onto banana stalk activated carbon. *Chem Eng J* 174:41–48. <https://doi.org/10.1016/j.cej.2011.08.026>
- Salman JM, Njoku VO, Hameed BH (2011b) Batch and fixed-bed adsorption of 2,4-dichlorophenoxyacetic acid onto oil palm frond activated carbon. *Chem Eng J* 174:33–40. <https://doi.org/10.1016/j.cej.2011.08.024>
- Salman-Naeem M, Javed S, Baheti V, Wiener J, Javed MU, Ul Hassan SZ, Mazari A, Naeem J (2018) Adsorption kinetics of acid red on activated carbon web prepared from acrylic fibrous waste. *Fibers and Polym* 19:71–81. <https://doi.org/10.1007/s12221-018-7189-5>
- Silverstein RM, Webster FX, Kiemle DJ (2005) Spectrometric identification of organic compounds. John Wiley & Sons, Inc.
- Souza AE, Teixeira SR, Santos GTA, Costa FB, Longo E (2011) Reuse of sugarcane bagasse ash (SCBA) to produce ceramic materials. *J Environ Manag* 92:2774–2780. <https://doi.org/10.1016/j.jenvman.2011.06.020>
- Sposito G (1998) On points of zero charge. *Environ Sci Technol* 32:2815–2819. <https://doi.org/10.1021/es9802347>
- Sriatun S, Taslimah T, Suyati L (2018) Synthesis of zeolite from sugarcane bagasse ash using cetyltrimethylammonium bromide as structure directing agent. *Indonesian J Chem* 18:159–165. <https://doi.org/10.22146/ijc.22197>
- Teixeira SR, de Souza AE, Santos GTA, Peña AFV, Miguel AG (2008) Sugarcane bagasse ash as a potential quartz replacement in red ceramic. *J Am Ceram Soc* 91:1883–1887. <https://doi.org/10.1111/j.1551-2916.2007.02212.x>
- Trivedi NS, Mandavgane SA, Kulkarni BD (2016) Mustard plant ash: a source of micronutrient and an adsorbent for removal of 2,4-dichlorophenoxyacetic acid. *Environ Sci Pollut Res* 23:20087–20099. <https://doi.org/10.1007/s11356-016-6202-7>
- Yan W, Liu D, Tan D, Yuan P, Chen M (2012) FTIR spectroscopy study of the structure changes of palygorskite under heating. *Spectrochim Acta Part A Mol Biomol Spectrosc* 97:1052–1057. <https://doi.org/10.1016/j.saa.2012.07.085>
- Yusof NH, Foo KY, Wilson LD, Hameed BH, Hazwan-Hussin M (2020) Microwave-Assisted Synthesis of Polyethyleneimine Grafted Chitosan Beads for the Adsorption of Acid Red 27. *J Polym Environ* 28:542–552. <https://doi.org/10.1007/s10924-019-01628-3>
- Zhang P, Liao W, Kumar A, Zhang Q, Ma H (2020) Characterization of sugarcane bagasse ash as a potential supplementary cementitious material: Comparison with coal combustion fly ash. *J Clean Prod* 277:123834. <https://doi.org/10.1016/j.jclepro.2020.123834>

Publisher's Note Springer Nature remains neutral with regard to jurisdictional claims in published maps and institutional affiliations.

Springer Nature or its licensor (e.g. a society or other partner) holds exclusive rights to this article under a publishing agreement with the author(s) or other rightsholder(s); author self-archiving of the accepted manuscript version of this article is solely governed by the terms of such publishing agreement and applicable law.